Supplementary Information for

Magnetism of Hypo-Oxide State at the Diffuse Internal Interface between Ferromagnet and Antiferromagnet

Min-Seung Jung[1], Mi-Young Im[2,3], Bong Ho Lee[4], Namkyu Kim[5], Ki-Suk Lee[5] and Jung-Il Hong[1,2]*

[1]Department of Emerging Materials Science, DGIST, Daegu 42988, Korea.

[2]Research Center for Emerging Materials, DGIST, Daegu 42988, Korea.

[3]Center for X-Ray Optics, Lawrence Berkeley National Laboratory, Berkeley, CA 94720, USA.

[4]Center for Core Research Facilities, DGIST, Daegu 42988, Korea.

[5]School of Materials Science and Engineering, KIST-UNIST Ulsan Center for Convergent Materials, UNIST, Ulsan 44919, Korea.

*Correspondence to: jihong@dgist.ac.kr

Hypo-oxide structure

Table S1 lists the average size of the grains in the films at different oxidation degrees obtained from the analyses of XRD peak widths (Fig. 1(a)). The grain sizes were obtained by using Scherrer equation: $d = \frac{0.96\lambda}{B\cos\theta}$, where λ is the wavelength of the X-ray (1.54 Å), B is the full width at half maximum (FWHM) and θ is the Bragg angle. From these results, both pure metallic and fully oxidized films have large grain sizes of ~10 nm. As the oxide phase concentration in the film increases, oxide grain size increases from 2 nm to 10 nm while the metal grain size decreases from 7 nm to 3 nm. In the case of the film with similar $Co_{0.7}Ni_{0.3}$ and $Co_{0.7}Ni_{0.3}O$ ratio, averaged grain size is about 3 nm. The film with 47.7 % oxide contents has the smallest grain size difference between FM ($Co_{0.7}Ni_{0.3}$) and AFM ($Co_{0.7}Ni_{0.3}O$) in comparison with other films, and it is expected that it would have the largest internal interface density among the series of specimens.

In order to investigate the detailed internal structure of the specimen, TEM investigation was also carried out with the mixed phase films. FIB technique was employed to prepare the sample for the cross sectional HR-TEM. TEM micrographs (Fig. S1) are consistent with XRD results. The grains in the pure metal and fully oxidized films exhibit distinctly different sizes from those in the mixed phase films with 47.7 % of oxidation degree. In other words, when the one phase is dominantly present in the film, the grains generally exhibit greater sizes, and individual grain is clearly distinguishable from neighboring grains. The grains of FM and AFM in the partially oxidized film are entangled with each other with complex geometrical distributions, and they are not clearly distinguishable from one another. Fig. S1(b)-(d) show the elemental mappings of different elements (oxygen, cobalt and nickel) in the films with various degrees of oxidation. Summing up the XRD and TEM results, metal and metal oxide phases with a few nm's of grain sizes are distributed without any spatial order, which leads to the amplified interface density.

We conducted first order reversal curve (FORC) measurement to identify magnetic phase in a 48 % oxidation mixture film which shows highest increase of saturation magnetization. The measurement is taken by measuring the minor hysteresis curves of the specimen with the applied magnetic field decreasing from saturation to a reversal field (H_a)

and then sweeping back a field (H_b) up to the saturation field repeatedly at various H_a. For the analysis of FORC distribution, second derivative magnetization was plotted as a function of (H_c, H_u) coordinates where coercive field (H_c) and interaction field (H_u) are obtained by $H_c = (H_b-H_a)/2$, $H_u = (H_b+H_a)/2$, respectively, as shown in Fig. S2. A single peak was confirmed in the plot suggesting the existence of one magnetic phase in the specimen. It is thought that exchange interaction is dominant and the composite film behaves as one magnetic phase rather than the mixture of multiple phases of various oxidation. Interaction field is observed to be shifted along the H_u axis, indicating strong exchange bias effect in the specimen.

The Co–CoO granular film series was also fabricated by using Co target under the identical conditions as those for the preparation of $Co_{0.7}Ni_{0.3}$-$Co_{0.7}Ni_{0.3}O$ film series. The Co-CoO mixture films were deposited on Si (400) wafer surfaces with native oxide layers by reactive sputtering at room temperature. The films were deposited at various oxygen gas contents in the atmosphere to prepare the varying degree of oxidation in the films.

Fig. S3 shows that fcc CoO peaks appear in the XRD patterns and their intensities sequentially increase with oxide contents in the films while the peaks corresponding to metallic hcp Co phase disappear gradually. As in the case with $Co_{0.7}Ni_{0.3}$-$Co_{0.7}Ni_{0.3}O$, when one phase (Co or CoO) dominates in the film, the FWHM of main peak decreases. It indicates that its grains are larger than those in the FM-AFM mixed phase. As shown in Table S2, the trend of grain size variation is similar to the trend for $Co_{0.7}Ni_{0.3}$- $Co_{0.7}Ni_{0.3}O$ film series.

TEM was carried out to identify the microstructural details of samples. Of the series of samples, films with 0 %, 43 %, and 82 % oxidation were examined. In consistence with the XRD results, as shown in Fig. S4, the grain size is smallest when metal and oxide phases are mixed. Co and CoO phases are confirmed in HR-TEM micrographs from the measurements of d-spacings based on the crystal structures and lattice parameters of Co and CoO. Selected area electron diffraction (SAED) patterns in cross-sectional TEM measurement (Fig. S4) were obtained, and the result was consistent with XRD. Diameter of the SA aperture is about 110 nm and the electron diffraction patterns were obtained without silicon substrate. With pure metal and fully oxidized films, the diffraction spots from the polycrystalline grains were recorded in the measured patterns. The SAED patterns

with 43 % oxide contents film mainly exhibit the diffraction rings consisting of small spots from Co and CoO phases. It indicates that the nano-grains of two phases are randomly distributed in the films without spatially preferred orientations.

Hysteresis loops of the Co–CoO mixture film with 43 % oxidation were also recorded in order to track the changes in magnetic properties (Fig. S5). In particular, the change of M_S values was noted in comparison with the results for $Co_{0.7}Ni_{0.3}$-$Co_{0.7}Ni_{0.3}O$ films. With Co-CoO mixture film with maximized interface density, as temperature increases from 10 K to 300 K, measured M_S varied by only 5 % from 839 emu/cm^3 to 885 emu/cm^3 while the change can be more than 25 % for the film of $Co_{0.7}Ni_{0.3}$ (52 %) - $Co_{0.7}Ni_{0.3}O$ (48 %). Increase of M_S up to ~300 K was followed by subsequent decrease upon further increase of the temperature.

In order to measure the atomic scale 3D structure of the internal interfaces, 43 % oxide contents film was fabricated into a tip shaped specimen employing the focused ion beam (FIB) and atom probe tomography (APT) was carried out. Movie S1 (attached in separate files) show 3D structural details of internal phase distributions obtained from APT results. Yellow surface represents the interface between metal and oxide phases. Both Co and CoO phase are mutually entangled with a few nm's of widths in all direction. Both phases do not form separate granules but are connected randomly to form network structures, which is beneficial to achieve maximized interface density with enhanced coupling interactions across the FM and AFM interfaces.

Considering all the structure analyses results as well as nearly identical film preparation procedures, $Co_{0.7}Ni_{0.3}$-$Co_{0.7}Ni_{0.3}O$ and Co-CoO are expected to have analogous structures.

Atomistic spin model simulations for AFM and FM interface

To investigate the temperature dependence of spin structure at the interface between antiferromagnet (AFM) and ferromagnet (FM), we modeled FM core surrounded by AFM shell (Fig. S7) by using VAMPIER code which utilizes a classical atomistic spin model with a Heisenberg spin Hamiltonian which describes the energetics of a FM core and AFM shell given by

$$H = H_{exchange} + H_{anisotropy} + H_{Zeeman}.$$

The exchange energy is

$$H_{exchange} = \frac{1}{2}\sum_{i \neq j} J_{ij} S_i \cdot S_j$$

where **S** is the spin unit vector, *i, j* label neighboring spin sites. J_{ij} is the exchange interaction between the atomic spin sites *i, j* with $J_{FM} = 12.2 \times 10^{-21}$ J/link and $J_{AFM} = -2.7 \times 10^{-21}$ J/link for the ferromagnetic and antiferromagnetic interactions, respectively. For the interfacial exchange coupling between FM and AFM, we assumed the same exchange interaction with J_{FM}. The single-ion uniaxial type anisotropy energy with the easy axis, e_z is given by:

$$H_{anisotropy} = K\sum_{i} (S_i \cdot e_z)^2$$

where the anisotropy constant $K = 4.644 \times 10^{-24}$ J/atom for both FM and AFM spins. The Zeeman energy by applied field, H_{app} is simply given by:

$$H_{Zeeman} = \mu_i S_i \cdot H_{app}$$

with magnetic moments μ_i = 1.72 and 1.0 Bohr magneton (μ_B) for FM and AFM sites, respectively.

As a model system, the FM sphere core with 3 nm-diameter located at the center of AFM cube with 5×5×5 nm^3 is used in our atomistic simulations. The crystal structure for both FM and AFM materials is face centered cubic (FCC) structure with the lattice constant of 2.5 Å. To simulate the temperature effects, the Monte Carlo Metropolis algorithm was adopted. The mean values of magnetic moments were obtained under the external field with 2 Tesla along the +*z* direction during more than 100 Monte Carlo calculation steps.

Figure S8 shows the representative spin configurations with mean value of M_S according to the temperature. At low temperature, FM spins in the core are tilted

considerably from the easy axis (*z*-axis) due to the interfacial coupling with AFM spins. As increasing the temperature, the thermal fluctuations of AFM spins become larger and thus, the interfacial coupling weaker effectively. Consequently, FM spins align further along the external field direction and the mean value of M_S increases with increasing temperature.

Figure S1.

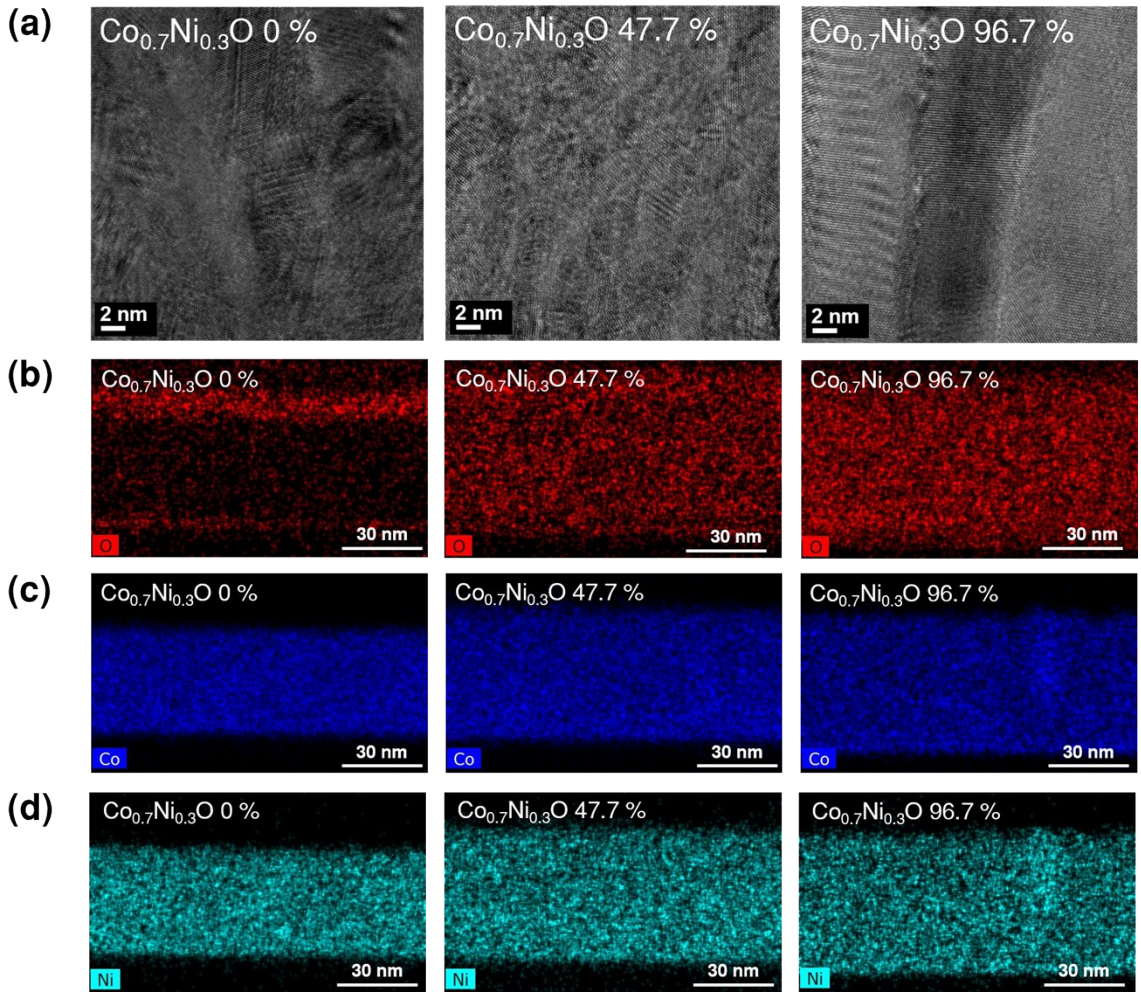

Fig. S1. High-resolution cross-sectional TEM micrographs and element mappings of the FM and AFM mixture films of 0 %, 47.7 % and 96.7 % oxidations. TEM micrographs are shown in (a) and elemental mappings for (b) Oxygen, (c) Cobalt, and (d) Nickel are shown.

Figure S2.

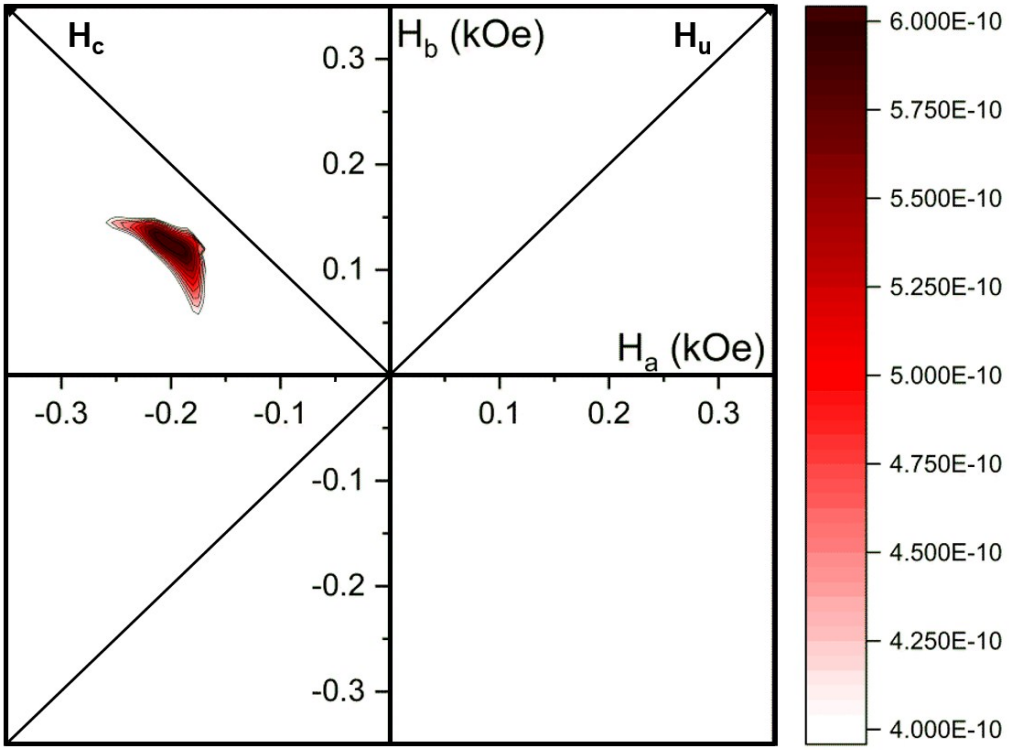

Fig. S2. FORC diagram with a 48 % oxidation of $Co_{0.7}Ni_{0.3}$- $Co_{0.7}Ni_{0.3}O$ mixture film.

Figure S3.

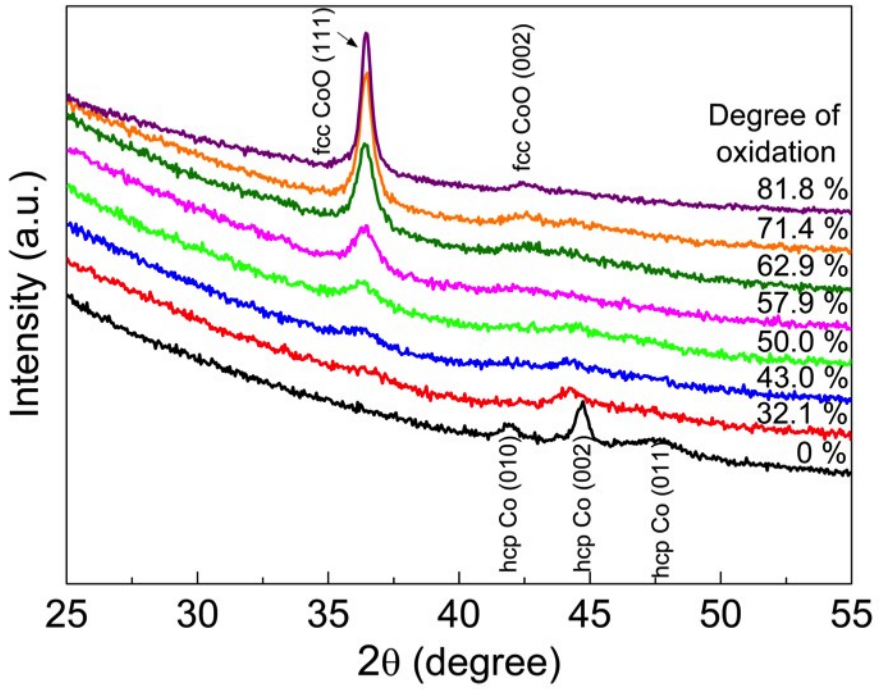

Fig. S3. XRD patterns of Co and CoO mixture film at various oxidation degrees.

Figure S4.

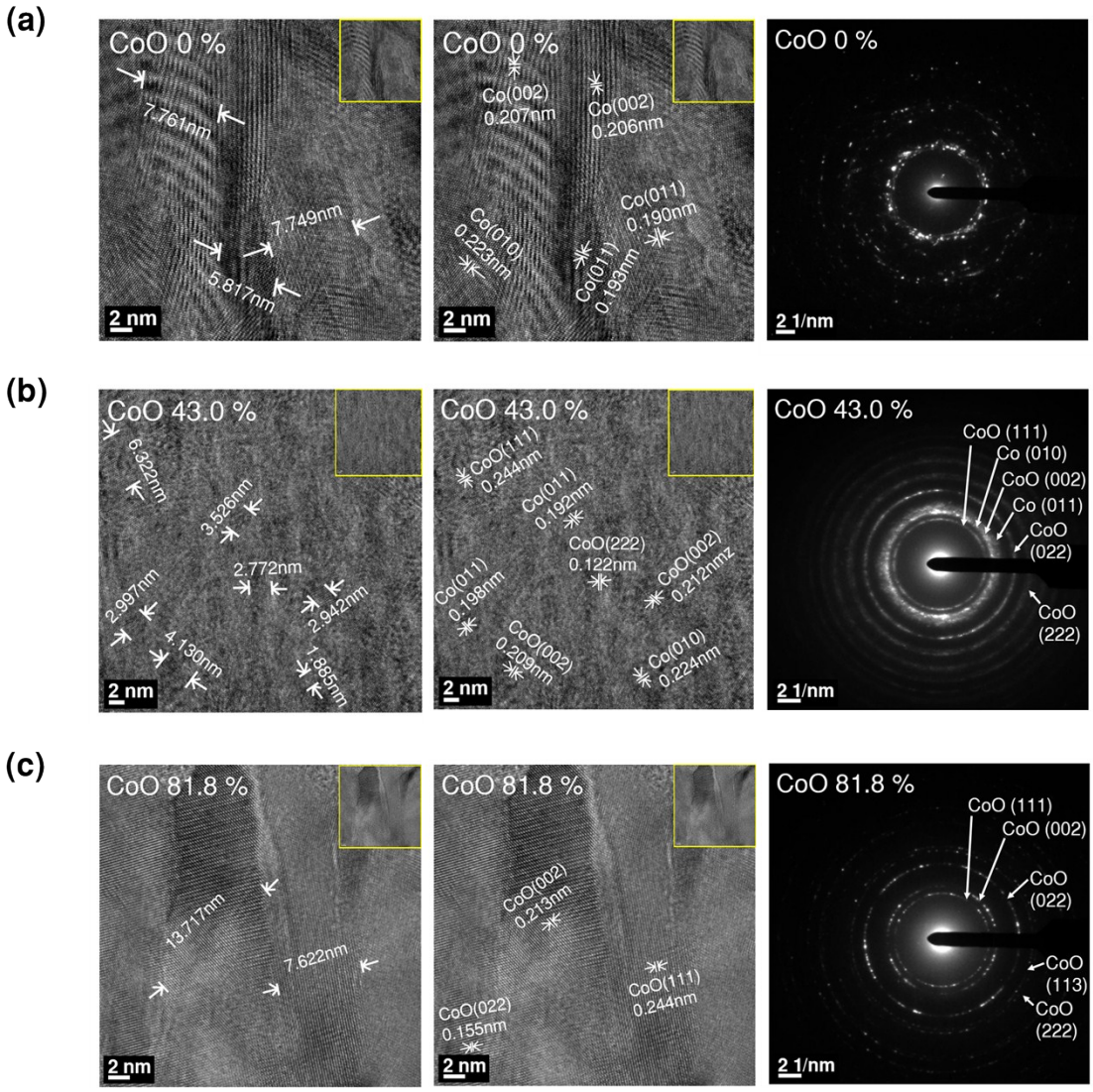

Fig. S4. High resolution cross-sectional TEM images and SAED patterns with Co and CoO phase mixtures. The degrees of oxidation in the films are (a) 0 %, (b) 43 % and (c) 81.8 %, respectively.

Figure S5.

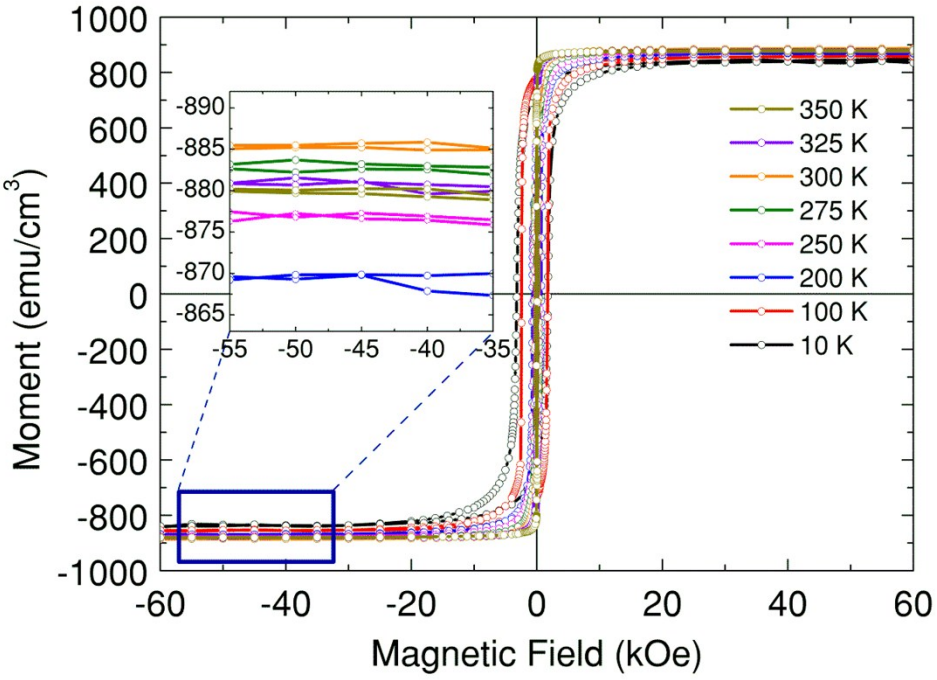

Fig. S5. Hysteresis loops of the film with 43 % oxidation measured at temperatures from 10 K to 350 K. Inset shows magnified view at high field region for a clearer observation of M_S change with temperature increase.

Figure S6.

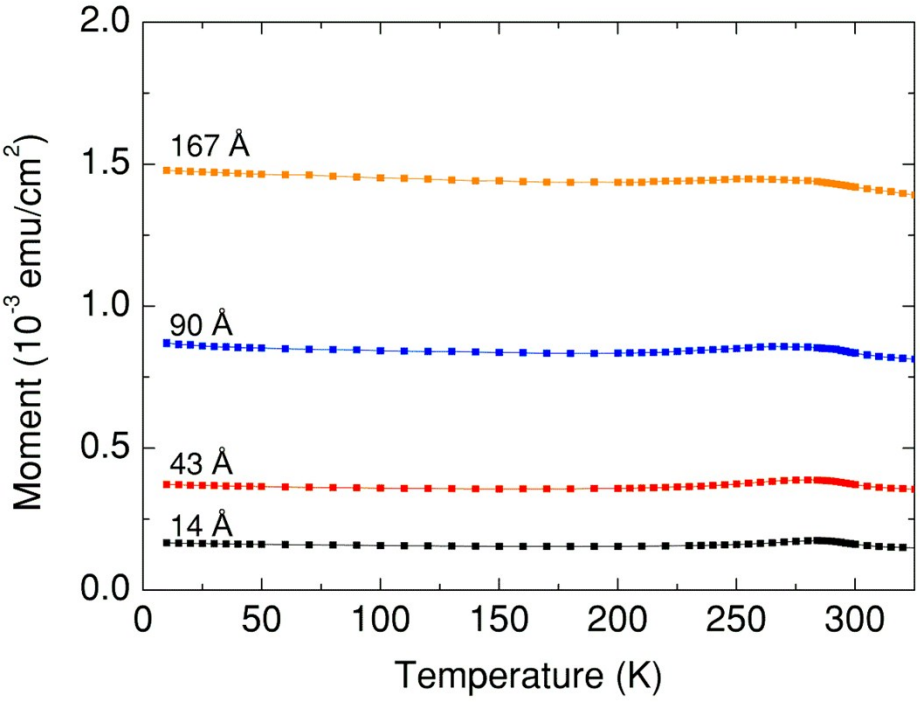

Fig. S6. Change of magnetic moment with temperature in the bilayer films of CoO (500 Å)/ $Ni_{0.8}Fe_{0.2}$ (t Å)/ SiO_2 (50 Å) with defined interface area. The thickness of FM layer (t) is 14 Å, 43 Å, 90 Å and 176 Å, respectively, as indicated in the figure.

Figure S7.

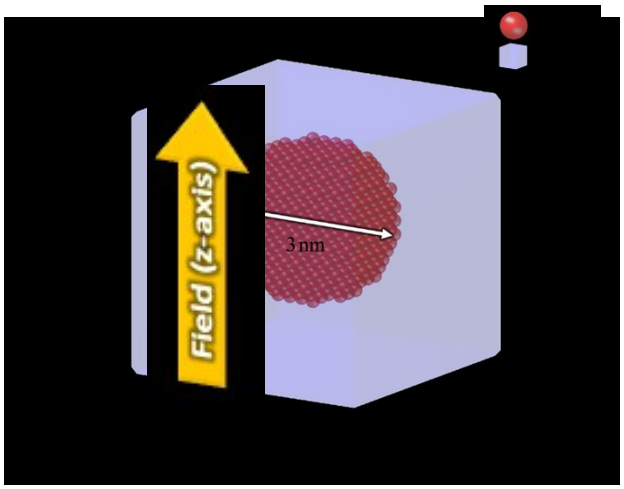

Fig. S7. Schematic diagram of the atomistic modeled core-shell structure. Red and blue regions represent the ferromagnetic (FM) and the antiferromagnetic (AFM) atoms, respectively.

Figure S8.

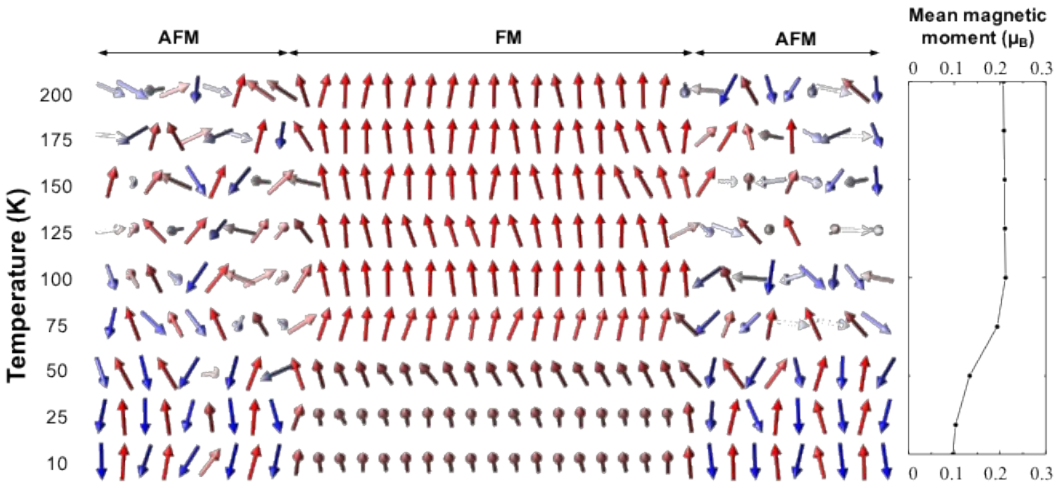

Fig. S8. Representative spin configurations along the crossing line through the AFM-FM region in the core-shell structure in Fig. S7 according to temperature and the plot of the values for mean magnetic moment for given temperature (right).

Table S1.

Table S1. The averaged grain size depending on the degree of oxidation in the $Co_{0.7}Ni_{0.3}$ and $Co_{0.7}Ni_{0.3}O$ mixture films estimated from the XRD results.

Oxide fraction (%)	Averaged $Co_{70}Ni_{30}$ grain size (nm)	Averaged $Co_{70}Ni_{30}O$ grain size (nm)
0	7.18	
31.9	3.29	1.82
47.7	3.27	2.96
53.9	3.15	2.54
57.9	3.48	2.98
67.8		3.62
77.0		6.01
77.7		5.17
96.7		9.68

Table S2.

Table S2. The averaged grain size depending on the degree of oxidation in the Co and CoO mixture films obtained from XRD results.

Oxide fraction (%)	Averaged Co grain size (nm)	Averaged CoO grain size (nm)
0	7.83	
32.1	4.41	2.68
43.0	3.55	3.02
50.0	2.25	4.06
57.9		4.47
62.9		6.04
71.4		7.85
81.8		10.28